

A SOLAR CORONAL JET EVENT TRIGGERS A CORONAL MASS EJECTION

JIAJIA LIU, YUMING WANG, CHENGLONG SHEN, KAI LIU, ZONGHAO PAN, AND S. WANG
 CAS Key Laboratory of Geospace Environment, Earth and Space Science School, University of Science and Technology of China,
 No. 96, JinZhai Road, Hefei, Anhui 230026, China

Received 2015 July 9; accepted 2015 October 4; published 2015 November 4

ABSTRACT

In this paper, we present multi-point, multi-wavelength observations and analysis of a solar coronal jet and coronal mass ejection (CME) event. Employing the GCS model, we obtained the real (three-dimensional) heliocentric distance and direction of the CME and found it to propagate at a high speed of over 1000 km s^{-1} . The jet erupted before the CME and shared the same source region. The temporal and spacial relationship between these two events lead us to the possibility that the jet triggered the CME and became its core. This scenario hold the promise of enriching our understanding of the triggering mechanism of CMEs and their relations to coronal large-scale jets. On the other hand, the magnetic field configuration of the source region observed by the *Solar Dynamics Observatory (SDO)*/HMI instrument along with the off-limb inverse Y-shaped configuration observed by *SDO/AIA* in the 171 \AA passband provide the first detailed observation of the three-dimensional reconnection process of a large-scale jet as simulated in Pariat et al. The eruption process of the jet highlights the importance of filament-like material during the eruption of not only small-scale X-ray jets, but likely also of large-scale EUV jets. Based on our observations and analysis, we propose the most probable mechanism for the whole event, with a blob structure overlaying the three-dimensional structure of the jet, to describe the interaction between the jet and the CME.

Key words: magnetic reconnection – Sun: activity – Sun: coronal mass ejections (CMEs)

Supporting material: animations

1. INTRODUCTION

As one of the most intriguing phenomena occurring in the solar atmosphere, solar jets have been studied extensively and deeply in the past few decades (e.g., Shibata et al. 1996; Cirtain et al. 2007; De Pontieu et al. 2007; Moore et al. 2010). Despite different properties in their dominant temperatures, scales, and dynamics, they are thought to be import for the release of solar magnetic free energy through reconnection (e.g., Shibata et al. 2007; Pariat et al. 2009; Fang et al. 2014; Liu et al. 2014) and to contribute to coronal heating and/or solar wind acceleration (e.g., Tsiropoula & Tziotziou 2004; Shibata et al. 2007; McIntosh et al. 2010; Liu et al. 2014). According to the numerical simulations in Pariat et al. (2009), the triggering mechanism of solar jets could be attributed to reconnection occurring within an inverse Y-shaped three-dimensional magnetic field configuration. However, direct observations of the detailed evolution of such three-dimensional (3D) reconnection are still absent.

Due to their significant effect on Earth’s environment, coronal mass ejections (CMEs) have attracted a great deal of attention since the beginning of the era of space physics (Low 2001, as a review). As a significant source of matter ejected from the Sun, CMEs have been studied thoroughly from several points of view: observational features (e.g., Wood et al. 1999), models (e.g., Priest & Forbes 1990; Lin & Forbes 2000), early evolution (e.g., Liu et al. 2014), interactions with each other (e.g., Shen et al. 2012), and their arrival at Earth (e.g., Shen et al. 2014). It is widely believed in the community that a substantial portion of CMEs are associated with prominence/filament eruptions (e.g., Gilbert et al. 2000; Gopalswamy et al. 2003).

What is hidden by the different typical geometries of jets (elongated) and CMEs (blob-like) are the distinct magnetic field configurations. While jets are usually believed to erupt

along open field lines (e.g., Shibata et al. 1996), CMEs are thought to be associated with closed helical fields (e.g., Chen et al. 1997). The potential relations and interactions between these two important phenomena (jets and CMEs) are intriguing and could enrich our knowledge of the various physical processes in the solar atmosphere. Previous studies have shown that some (narrow) CMEs could be extensions of large-scale solar jets in white-light coronagraphs (e.g., Wang et al. 1998; Liu 2008). Another possibility is that one of them might be triggered by the other. However, do these possibilities truly exist in the solar atmosphere? How does such an interaction between a CME and a jet occur? Corresponding observations and analysis have not yet been performed.

In this paper, we present multi-point, multi-wavelength observations and analysis of a jet and CME event. The jet originated from a single positive polarity active region, driven by a 3D magnetic topology which surprisingly resembled that in Pariat et al. (2009), providing the first detailed observations of the evolution of such a 3D-reconnection triggering mechanism for solar jets. The CME is found to be triggered by the jet event with the jet becoming its core, illustrating a scenario in which these two eruptive events could be closely related. We present our conclusions in Section 4 based on the observations in Section 2 and our discussion in Section 3.

2. OBSERVATIONS

During the (quasi-) frontal travel of active region NOAA 11644 (Figure 1(C)), it displayed several attractive eruptions, the most intriguing of which is the one occurring after 19:00 UT on 2013 January 15. A fast CME with a speed of over 1000 km s^{-1} was observed simultaneously by the coronagraphs LASCO C2/C3 on board the *Solar and Heliospheric Observatory (SOHO)* and COR1/COR2 on board both probes of the *Solar TERrestrial Relations Observatory (STEREO)*;

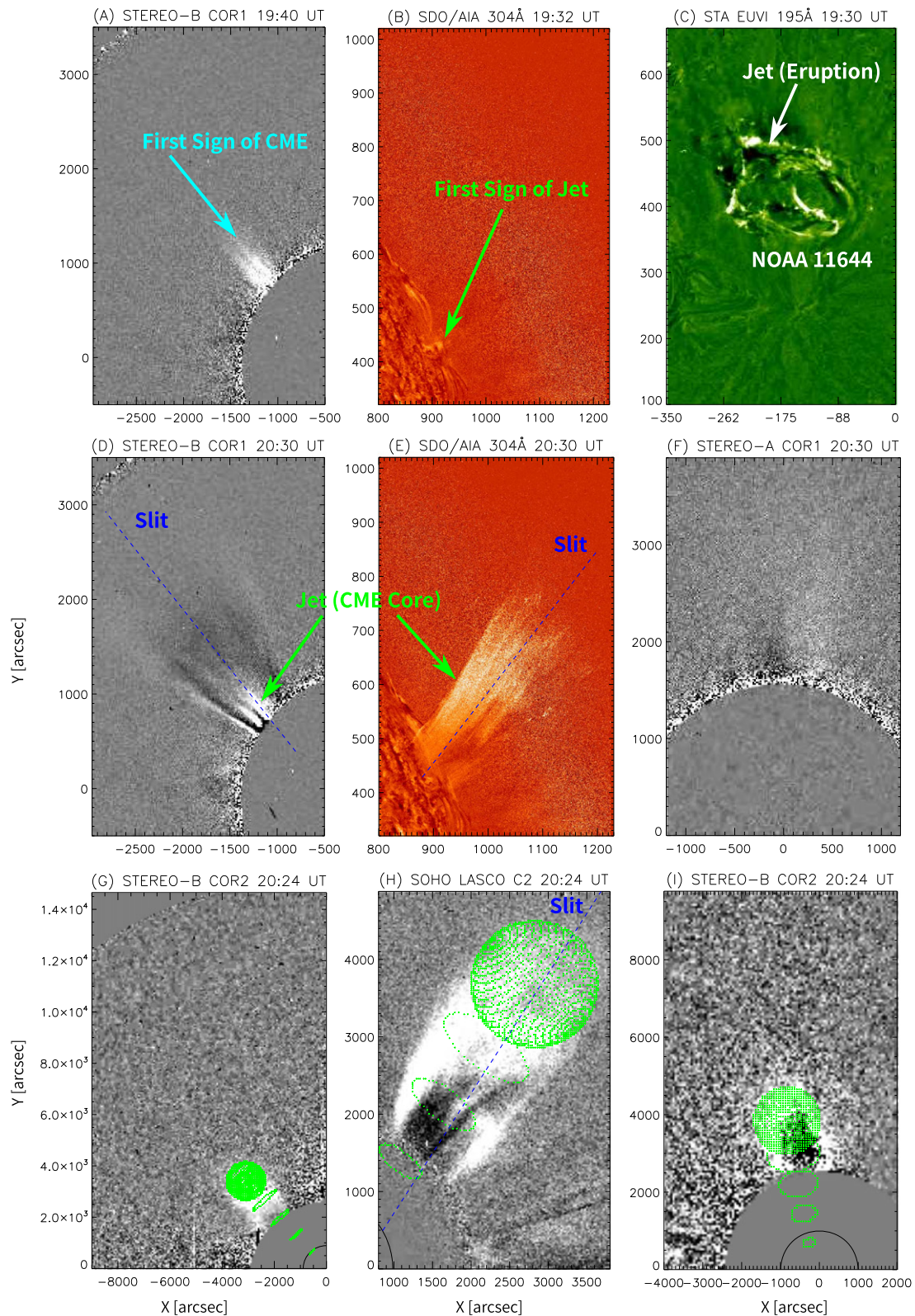


Figure 1. Multi-point observations of the jet and CME by *SDO* AIA, *SOHO* LASCO, and *STEREO* EUVI/COR1/COR2. The top three panels are the *STEREO-B* COR1 observations of the first sign of the CME at 19:40 UT, the *SDO* AIA 304 Å observations of the first sign of the jet at 19:32 UT and the *STEREO-A* EUVI 195 Å observations of the source region of the jet (active region NOAA 11644) at 19:30 UT, respectively. The middle three panels are the *STEREO-A/B* COR1 and *SDO* AIA 304 Å passband observations at the same time 20:30 UT. The slits are selected along the axial direction of the jet or CME. The bottom three panels are the simultaneous observations by the *STEREO-A/B* COR2 and *SOHO* LASCO C2 instruments of the CME on 20:24 UT. The green dotted wires are the resulting surface of the reconstructed structure of the CME employing the GCS forward modeling method (see descriptions of the model in the text and more in Themisien et al. 2009). (Animations a, b, and c of this figure are available.)

Kaiser et al. 2008; Figure 1, animation M1). Just before the CME, a solar coronal EUV jet was observed in the fields of view (FOV) of the AIA instrument on board the *Solar Dynamics Observatory* (*SDO*; Pesnell et al. 2012) and the EUVI instruments on board both of the *STEREO* probes (Figure 1, animation M2). Figure 1(B) and (C), together with animation M2, show great temporal agreement between the observed jet via *SDO* AIA and the eruption activities within active region NOAA 11644 via *STEREO-A* EUVI, indicating that the active region should be the source region of the jet. The location of the center of the active region was about E10°N24° in the FOV of the *STEREO-A* EUVI instrument. As *STEREO-A* was about 129° ahead of Earth (and *SDO* and *SOHO*) at 19:00 UT, the longitude of the center of the active region seen from *SDO* should be W119°.

The CME appeared on the north-east limb around 19:40 UT in the FOV of *STEREO-B* (STB) COR1 (Figure 1(A)), which was about 134° behind Earth (and *SOHO* and *SDO*). The coronagraph LASCO C2 captured the first image of the CME at around 20:00 UT and half an hour later LASCO C3 and *STEREO* COR2 captured images. To obtain the 3D (real) direction, position, and velocity of the CME, we employ a forward reconstruction model (the GCS model) proposed by Thernisien et al. (2009), which assumes a self-similar expanding flux rope structure for the target CME. We then compare the resulting flux rope obtained from the GCS model with the images from LASCO C2/C3 and STA/STB COR2 at six instances when we could at least partially identify the leading edge of the CME in all three images (from LASCO C2, STA COR2, and STB COR2), to obtain the best agreement between the flux rope and the CME. The parameters of the flux rope could tell us the actual height (heliocentric distance), longitude, and latitude, of the CME at different times. One set at 20:30 UT is shown in panels (G)–(I) in Figure 1 where the green dotted wires are the surface of the flux rope structure.

The results demonstrate that the latitudes and longitudes of the CME remained almost constant around N48° and W120° seen from Earth (and *SDO*) throughout its travel from 6 Rs to 20 Rs. A parabolic fit between the heliocentric distance of the CMEs leading edge and the corresponding time shows an average propagation speed of the CME around 1031 km s^{-1} .

On the other hand, we observe continuous small brightenings starting at 19:16 UT in the AIA 304 Å passband images around N24° at the north–west limb and the first sign of plasma eruption forming a jet around 19:32 UT (Figure 1(B), animations M2 and M3), a few minutes before the CME appeared in the FOV of the *STEREO* COR1 observations (19:40 UT). Most of the jet materials were seen in the AIA 304 Å passband and were rarely found in passbands with characteristic temperature above 2 MK (211 Å, Lemen et al. 2012), indicating that the jet was primarily formed with chromospheric cool materials (online movie M2). The jet continued to rise along a trajectory that was approximately 28° counter-clockwise away from the local radial direction and did not show any sign of falling back. The position angle of the jet was almost the same as that of the CME (animation M1).

The similarity in position and the temporal relationship between the jet and CME suggests that there should be some close relations between them: (1) the CME was the outer manifestation of the jet in the coronagraphs, (2) the CME was a bulk of materials that was triggered by the jet event, and (3) the lifting of the CME blob triggered footpoint region activity and

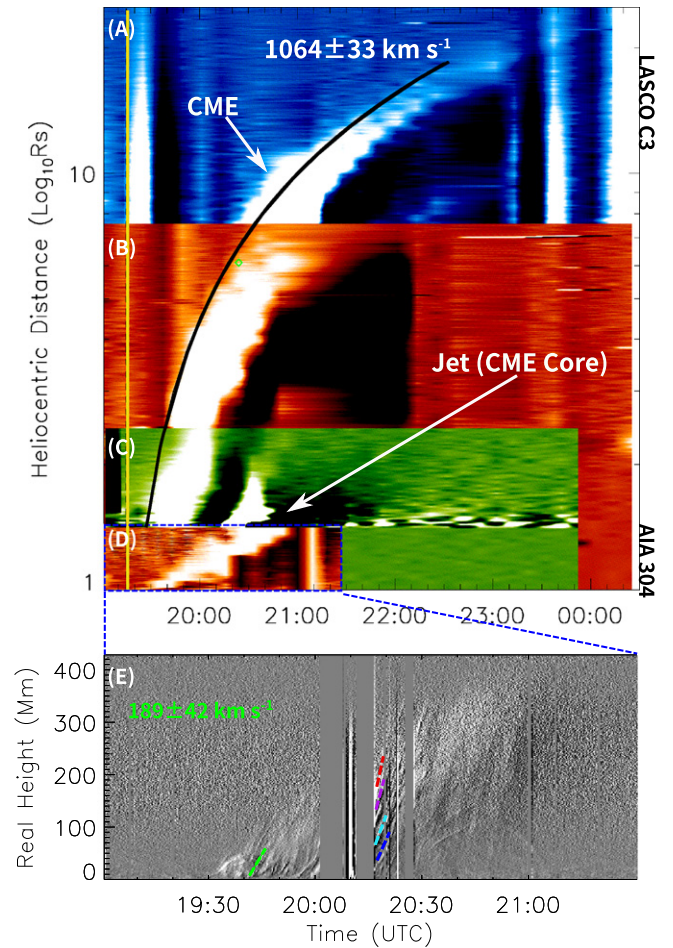


Figure 2. Panels (A)–(C): running-difference time–distance plots of the slits shown in Figure 1 based on data from *SOHO* LASCO C3, C2, and *STEREO-B* COR1, respectively. Panels (D)–(E): running-difference time–distance plots of the cadence-reduced and original *SDO* AIA 304 Å passband data, respectively. The yellow vertical line across panels (A)–(D) indicates the time when the first brightening occurred at 19:16 UT inside the source region of the jet. The black solid curve across panels (A)–(C) shows the fitted leading edge of the CME with a linear fit which results in an average speed of 1064 km s^{-1} . The green diamond shown in panel (B) is the leading edge reconstructed via the GCS model at 20:24 UT in panels (D)–(F) in Figure 1. Color-coded lines in panel (E) give examples of the tracks and velocities of different sub-jets.

the eruption of the jet. The third point could be directly excluded because the activities which triggered the jet were more than 20 minute earlier than when the CME was observed in the FOV of STB COR1 (19:16 UT versus 19:40 UT). To determine which of the first two situations is true, we placed a slit along the CME direction in the STB COR1 images (Figure 1(D)), a slit along the jet axis in the AIA images (Figure 1(E)), and a slit along the CME direction in the LASCO C2/C3 images (Figure 1(H)), which was the extension of the slit in the AIA images. The corresponding time–distance plots are shown in Figure 2 with the projection effect corrected based on the GCS result.

Obviously, the CME could be found in all three running-difference time–distance diagrams for STB COR1 (Figure 2(C)) and LASCO C2/C3 (Figures 2(A) and (B)) and they show very high consistency. Fitting the leading edge of the CME in the time–distance plots of these coronagraphs via a linear function yields an average velocity of about $1064 \pm 33 \text{ km s}^{-1}$, which is highly consistent with the GCS result

(1031 km s⁻¹). Figure 2(D) shows the corresponding running-difference time–distance plot of the AIA 304 Å images with a deduced cadence of 10 minutes to make it comparable to the STB COR1 plot. It is shown that there was no clear manifestation of the CME in the AIA 304 Å observations (or in the other EUV passbands of AIA, which is not shown here; see animation M2). Also, the time sequence shows that the CME was not the extension of the jet in the coronagraphs.

High-cadence (12 s) AIA images may provide us with some detailed kinetics of the jet. Figure 2(E) shows the de-projected running-difference time–distance plot along the slit in Figure 1(E) using the 12 s-cadence images of the AIA 304 Å passband. Sub-jets were expelled successively, indicating that continuous reconnection occurred around the source region of the jet as described in Moore et al. (2010) and observed in Liu et al. (2014). The average axial speed of these sub-jets was about 189 ± 42 km s⁻¹ at the bottom (green dashed line in Figure 2(E)) and they could be found to undergo obvious acceleration. However, it is difficult for us to trace the track of a particular sub-jet in the time–distance plot in order to estimate the exact acceleration due to the 20 minute data gap from about 20:01 UT. The speed of the jet in the FOV of STB COR1 was found to be almost the same as that of the CME’s leading edge which, together with the great continuity between the AIA plot and coronagraph plots, indicates that the CME was triggered by the jet event with the jet becoming its core, in agreement with the second relation above.

3. MECHANISMS AND DISCUSSIONS

The source region of the jet identified as active region NOAA 11644 can clearly be seen in *STEREO-A* EUVI 195 Å observations. Figures 3(A)–(D) exhibit four different times before, during, and after the eruption. Figure 3(A) shows the active region before the eruption at 19:00 UT, with the red–blue contours representing the line-of-sight (LOS) photospheric magnetic fields observed by the HMI instrument on board *SDO* at 17:00 UT nine days earlier when the active region was almost facing the satellite. It is clearly shown that the active region contained a single positive polarity surrounded by negative polarities, with another positive polarity at the lower left in a southern active region. Filament-like materials marked as a purple dashed curve could be found around the polarity inversion region between the single positive polarity and the surrounding negatives. Brightenings began around 19:15 UT, as shown in panel (B), and developed into the jet eruption which was seemingly formed by filament-like materials. The eruption began near the left end of the purple curve, gradually proceeded clockwise, and rooted near the right end, as shown in panel (C). Newly formed loops could also be observed after the eruption of the jet, exhibited in panel (D). As we can see from animation 2 and Figure 3, the filament-like materials participated significantly in the triggering process and finally formed the erupted jet.

Figure 3(E) shows the AIA 171 Å observations at 08:00 UT one day before the event and not long after the active region turned to the limb. Images in the 171 Å passband can mostly resolve the magnetic field topology in the lower corona and show a clear inverse Y-shaped configuration (enclosed in the red dashed rectangle in Figure 3(E)), which almost kept pace exactly with the simulations of solar jets in Pariat et al. (2009) and seems similar to the magnified “anemone” jet’s root as observed in Shibata et al. (2007). The photospheric magnetic

field, the off-limb inverse Y-shaped configuration, the eruption process of the jet material, and the existence of newly formed loops after the eruption are very similar to the 3D-reconnection simulations in Pariat et al. (2009), leading us to surmise that similar 3D reconnections are happening in this particular event.

Based on the above observation and analysis, we are able to propose the most probable mechanism for the whole event, which is shown as a two-dimensional (2D) sketch in Figure 4. Periphery field lines that originate from the single positive polarity inside active region 11644 and end at the negative polarities form the inner fan (green fields in Figure 4). Among these are the bottom fields of the CME (cyan fields) originating from the southern positive polarity. If activities underneath the inner fields introduce any twist/shearing (shown as the blue field), then magnetic free energy will build up and reconnection will occur when the balance is broken (Pariat et al. 2009; Fang et al. 2014). Plasma materials that speed up through the reconnection will then form a jet (gray-colored arrow). The bursts could also provide a push to the blob structure on the black dashed horizontal line. Due to the lack of observations of the early stage of the blob structure, we cannot know how the bursts pushed it in this particular event. Several effects, such as (1) the elevated inner fan due to the reconnections (Pariat et al. 2009) or/and (2) the accelerated jet materials, could lead to the ascension of the blob. Under the effect of one or more of the above processes, the blob rises and forms the observed CME.

Similar to the event modeled in Fang et al. (2014) and that observed in Liu et al. (2014), the rotational motions of the jet’s material could also be observed from the AIA 304 Å images in this event. Slits placed perpendicular to the jet’s axis (not shown in the figures) allow us to estimate the rotating periods of the materials employing a sine-function fit as in Liu et al. (2014). Periods turn out to be about 15 minutes at the bottom with a resulting linear speed of about 280 km s⁻¹. The periods became longer at the top of the jet in the FOV of AIA, indicating a deceleration of the rotational motion. As illustrated in Liu et al. (2014), the rotational motion arises with the release of residual magnetic free energy after reconnection; the amount of the residual would affect the rotational motion of the jet. Thus, it is possible that in this particular case, the reconnection may have already released most of the magnetic free energy and little is left to drive the rotational motion.

However, another situation in which the angular momentum of the jet passes into that of the CME is not prohibited. Considering the lack of direct observations of the rotational motion of the CME (discussions on this particular issue can be found in Tian et al. 2013, for example), we could try to figure out whether or not this situation is possible based on the poloidal motion of the magnetic clouds (MCs), which are the counterparts of CMEs in interplanetary space. As derived from a velocity-modified cylindrical force-free flux rope model based on Wind observations, Wang et al. (2015) found that almost all MCs more or less had shown poloidal motion with a meridian linear speed of around 10 km s⁻¹ (50% are below to km s⁻¹). Assuming that all of the angular momentum of the jet has passed to the CME, a self-expanding propagation of the CME and conservation of the angular momentum in the interplanetary space, the poloidal speed of the MC, evolved from the CME in this particular case, would be about 1.3 km s⁻¹, which is not prohibited by the observations in Wang et al. (2015).

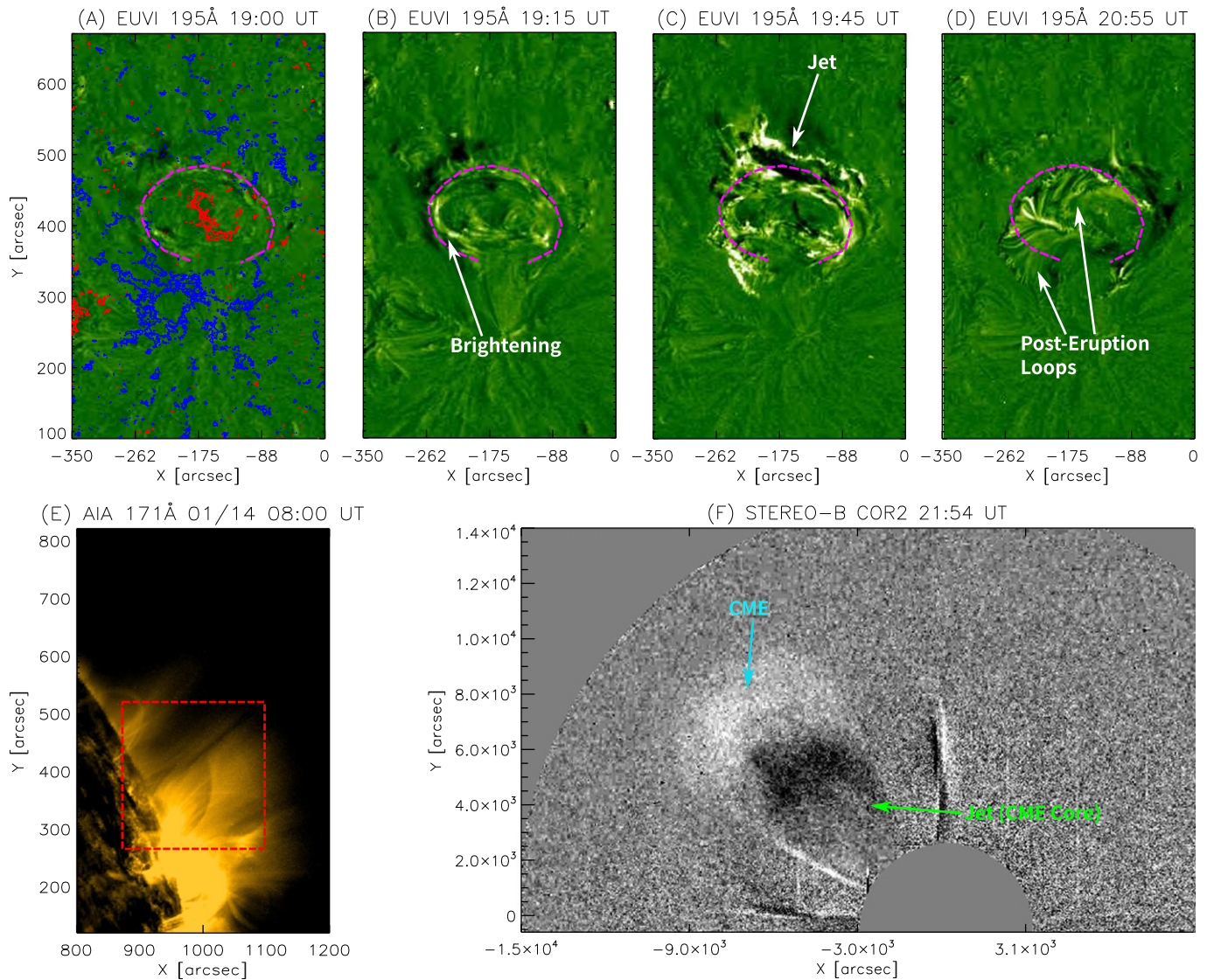


Figure 3. Panel (A)–(D): time-sequence evolution of the source region (NOAA 11644) of the jet and the CME in the FOV of the *STEREO-A* EUVI 195 Å passband. The red and blue contours in (A) show the positive and negative magnetic fields observed by the *SDO* HMI instrument nine days before the jet and CME event. The purple dashed curve marks the filament-like materials around the polarity inversion region before the eruption. Panel (E) is the *SDO* AIA 171 Å image at 08:00 UT one day before the event, resolving an inverse Y-shaped configuration of the magnetic field lines enclosed in the red dashed rectangle. Panel (F): *STEREO-B* COR2 observation on the CME and the jet (CME core) at 21:54 UT.

4. CONCLUSIONS

In this paper, we present our analysis of a coronal jet and a related CME, employing multi-wavelength, multi-point observations from *SDO* AIA/HMI, *STEREO* EUVI/COR1/COR2, and *SOHO* LASCO C2/C3.

Detailed analysis has shown that there is a close relationship between the jet and the CME. Employing the GCS reconstruction model, we are able to obtain the actual heights and positions of the CME at different times. We find that the CME propagated with a speed of over 1000 km s^{-1} . After correcting for the projection effect using the results from the GCS model, we plot the time–distance diagrams of the CME in the FOV of STB/COR1 and LASCO C2/C3, and of the jet in the FOV of *SDO*/AIA. We show that the CME was not the extension of the jet in the coronagraphs, but was triggered by the jet event with the jet becoming its core. All of the observations indicate that a (high-speed) CME could also be triggered by a jet event underneath, which is quite different from classical models (e.g.,

Lin & Forbes 2000) and provides a new viewpoint from which to study the relations between these two different mass release events in the solar atmosphere.

The jet originated from a source region with a single positive polarity surrounded by negative polarities. All of the observational features and their source region configuration proved to be highly consistent with the 3D reconnection simulation of solar jets in Pariat et al. (2009), providing the first detailed observations of such 3D reconnection triggering processes in large-scale EUV jets. The erupting process of the jet observed by the *STEREO-A* 194 Å instrument highlights the importance of the footpoint region filament-like materials in precipitating the eruption, which might provide additional evidence to the model proposed by Sterling et al. (2015; in which the authors showed evidence for X-ray small-scale jets).

The rotational motion of the jet materials could also be observed in the AIA 304 Å images. The rotational motion was found to decelerate. The deceleration could either be caused by

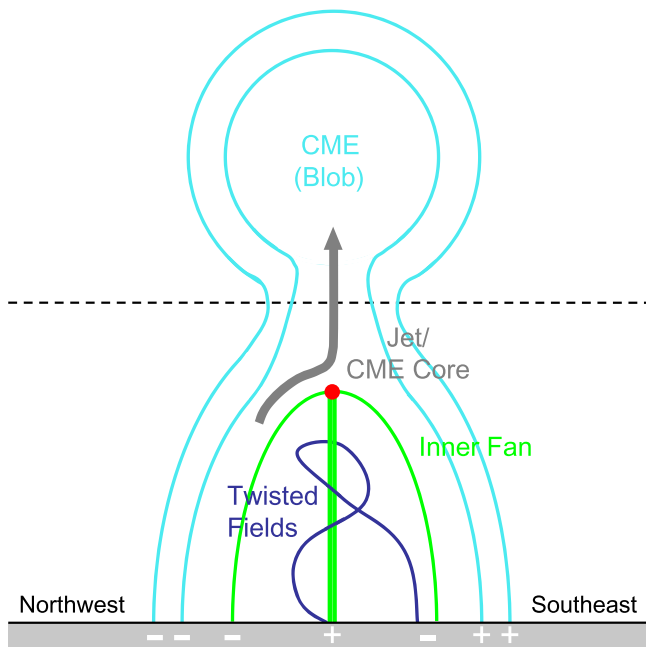


Figure 4. 2D sketch version of the magnetic field configuration that results in the observed event and phenomena. See the text for details of the illustration on the mechanisms.

(1) little magnetic free energy remaining after the reconnection, or/and (2) the angular momentum of the jet passing to the CME. Due to the lack of observations of the temporal magnetic fields and early stages of the CME, and a lack of in situ data, we cannot exclude either of these two explanations. On the other hand, as the CME was invisible in the observations of the AIA instrument due to the different temperature or/and the submarginal height, we are not able to figure out how exactly the CME interacted with the underlying jet event. This made the physical image incomplete to describe the interactions between the CME and the jet event of our picture in Figure 4. Future work with further observations and additional numerical simulations may shed light on the issues raised above.

We acknowledge the use of data from the *Solar Dynamics Observatory (SDO)*, the *Solar TERrestrial RELations*

Observatory (STEREO) and the *Solar and Heliospheric Observatory (SOHO)*. Animation M1 was generated using the “JHelioviewer” tool (<http://www.helioviewer.org>). This work is supported by grants from NSFC (41131065, 41121003, and 41574165), CAS (Key Research Program KZZD-EW-01-4), MOST 973 key project (2011CB811403), MOEC (20113402110001), and the fundamental research funds for the central universities. The research leading to these results has also received funding from NSFC 41274173, 41404134 and 41304145.

REFERENCES

- Chen, J., Howard, R. A., Brueckner, G. E., et al. 1997, *ApJL*, 490, L191
 Cirtain, J. W., Golub, L., Lundquist, L., et al. 2007, *Sci*, 318, 1580
 De Pontieu, B., McIntosh, S., Hansteen, V. H., et al. 2007, *PASJ*, 59, 655
 Fang, F., Fan, Y., & McIntosh, S. W. 2014, *ApJL*, 789, L19
 Gilbert, H. R., Holzer, T. E., Burkepile, J. T., & Hundhausen, A. J. 2000, *ApJ*, 537, 503
 Gopalswamy, N., Shimojo, M., Lu, W., et al. 2003, *ApJ*, 586, 562
 Kaiser, M. L., Kucera, T. A., Davila, J. M., et al. 2008, *SSRv*, 136, 5
 Lemen, J. R., Title, A. M., Akin, D. J., et al. 2012, *SoPh*, 275, 17
 Lin, J., & Forbes, T. G. 2000, *JGR*, 105, 2375
 Liu, J., Wang, Y., Liu, R., et al. 2014, *ApJ*, 782, 94
 Liu, R., Wang, Y., & Shen, C. 2014, *ApJ*, 797, 37
 Liu, Y., 2008, *SoPh*, 249, 75
 Low, B. C. 2001, *JGRA*, 106, 25
 McIntosh, S. W., Innes, D. E., de Pontieu, B., & Leamon, R. J. 2010, *A&A*, 510, L2
 Moore, R. L., Cirtain, J. W., Sterling, A. C., & Falconer, D. A. 2010, *ApJ*, 720, 757
 Pariat, E., Antiochos, S. K., & DeVore, C. R. 2009, *ApJ*, 691, 61
 Pesnell, W. D., Thompson, B. J., & Chamberlin, P. C. 2012, *SoPh*, 275, 3
 Priest, E. R., & Forbes, T. G. 1990, *SoPh*, 126, 319
 Shen, C., Wang, Y., Pan, Z., et al. 2014, *JGRA*, 119, 5107
 Shen, C., Wang, Y., Wang, S., et al. 2012, *NatPh*, 8, 923
 Shibata, K., Nakamura, T., Matsumoto, T., et al. 2007, *Sci*, 318, 1591
 Shibata, K., Shimojo, M., Yokoyama, T., & Ohyama, M. 1996, in ASP Conf. Ser. 111, Theory and Observations of X-Ray Jets (San Francisco, CA: ASP), 29
 Sterling, A. C., Moore, R. L., Falconer, D. A., & Adams, M. 2015, *Natur*, 523, 437
 Thernisien, A., Vourlidas, A., & Howard, R. A. 2009, *SoPh*, 256, 111
 Tian, H., Tomczyk, S., McIntosh, S. W., et al. 2013, *SoPh*, 288, 637
 Tsiropoula, G., & Tziotziou, K. 2004, *A&A*, 424, 279
 Wang, Y., Zhou, Z., Shen, C., Liu, R., & Wang, S. 2015, *JGR*, 120, 1543
 Wang, Y.-M., Sheeley, N. R., Jr., Socker, D. G., et al. 1998, *ApJ*, 508, 899
 Wood, B. E., Karovska, M., Chen, J., et al. 1999, *ApJ*, 512, 484